Validation of stereo vision based liver surface reconstruction for image guided surgery

Teatini Andrea[1,3]*, Wang Congcong[2]*, Palomar Rafael[1,2], Alaya Cheikh Faouzi[2], Beghdadi Azeddine[4], Edwin Bjørn[1,5], Elle Ole Jakob[1,3]

[1] *The Intervention Centre, Oslo University Hospital, Oslo, Norway.*
[2] *Norwegian Colour and Visual Computing Lab, Norwegian University of Science and Technology, Gjøvik, Norway.*
[3] *Department of Informatics, University of Oslo, Oslo, Norway*
[4] *L2TI-Institut Galilée, Université Paris 13, Sorbonne Paris Cité, Villetaneuse, France*
[5] *Oslo University Hospital, Department of Hepato-Pancreatic-Biliary surgery, Oslo, Norway*

Abstract—**Image guided surgery systems aim to provide navigation to surgeons in order to improve accuracy and safety of the procedures. Through stereo reconstruction algorithms, it is possible to generate 3D surfaces intra-operatively by means of a laparoscopic stereo-camera. This study aims to setup a simulation system and quantitatively validate a recent proposed reconstruction algorithm with application to laparoscopic liver resection surgery. The intra-operative surface will be used to guide model to patient registration. This will also improve accuracy of the navigation by correcting intra-operative deformations of the liver, such as those due to pneumoperitoneum. The accuracy results of the reconstruction method was found to be 3.7±0.8 mm in terms of Hausdorff distance. The validation therefore indicates the feasibility and accuracy of the surface reconstruction method.**

1. Introduction

Image guided surgery utilizes computer based techniques to provide imaging and navigation throughout medical procedures to support surgeons [1], [2]. In the past decade, with the technological advances in computer science and medical imaging, image guided surgery has greatly expanded.

The image guidance is based on a combination of medical images, such as Magnetic Resonance Imaging (MRI) or Computed Tomography (CT) and instrument tracking for surgical instruments. This information is displayed to surgeons either through Augmented Reality (AR) or through separate monitors. Image guided surgery is however complicated by the fact that most volumetric images are acquired pre-operatively. This is a problem especially within the field of laparoscopic surgery, where inflation of the patient's abdomen is performed. Pneumoperitoneum is, in fact, necessary to have enough space in the abdomen to visualize the patient's organs through the laparoscope camera, however, the inflation also deforms the shape of the organs [3]. This

leads to less accurate image guidance, which could also cause misinterpretation of the anatomical structures. Hence, update of pre-operative organ models through intra-operative imaging, such as stereo-laparoscopy, is necessary to account for these deformations.

In order to improve the depth perception to account for loss of haptic feedback due to laparoscopic surgery, stereo laparoscopes have been introduced into modern surgery. Stereo-cameras can not only provide better depth perception, but also provide information to reconstruct volumetric data (surface reconstruction) through computer vision techniques. Surface reconstruction in computer vision has also been performed using techniques such as Time-of-Flight (ToF) and Structured Light (SL), however, stereo-vision has the benefit of not introducing new hardware to surgery. Moreover, stereo surface reconstruction is more accurate with respect to monocular vision based reconstruction methods [4], [5].

Image guided surgery based on stereo vision has been researched for decades with various application fields, such as heart surface reconstruction to abdominal soft tissue reconstruction [6]–[8]. Simulation systems and test datasets are available in the literature to perform quantitative evaluations of reconstruction algorithms. In [9], Maier-Hein *et al.* present a comparative study of different organ reconstruction methods under their simulation environment and the dataset is public available. In [10], Suwelack *et al.* made publicly available their dataset to test their liver registration method. In [11], a validation of image guided liver laparoscopic system is presented. In [12], Heiselman *et al.* created a laparoscopic environment based on an abdominal phantom system, aiming for a quantitative assess registration accuracy. Nonetheless, although some datasets are available for the evaluation of surface reconstruction or registration, the datasets are valid only for their specific experimental setup. In [8], testing of the reconstruction method was performed based on datasets available online. However, to explore the validity of proposed algorithms in a more realistic scenario, validation also needs to be performed in a simulation setup which reproduces the desired application of the algorithm.

In this paper, both a simulation setup for laparoscopic liver surgery and a validation procedure of a recently published surface reconstruction method are presented. The purpose of this study was to: (1) setup a simulation system to quantitatively evaluate liver surface reconstruction and registration algorithms for stereo laparoscopic surgery; (2) quantitatively evaluate the liver surface reconstruction method proposed in [8].

The structure of this paper is organized as follows: Section 2 describes the experimental setup and introduces the methods used to perform the validation. Section 3 presents the results of the experiments. Section 4 is the discussion of the results of this study. Section 5 describes the conclusions and future works.

2. Materials and Methods

The workflow for validation of the reconstruction method is shown in Fig. 1. The validation was performed using a liver phantom model based on real human anatomy. The steps performed for validation and evaluation of the reconstruction method were based on the conventional approach for planned liver laparoscopic resection surgery. Initially, a pre-operative 3D segmentation model was created from a CT scan, thereafter, an intra-operative 3D surface reconstruction from stereo laparoscope was acquired, and finally registration between the two surfaces was performed. CT imaging of the liver phantom was used as ground truth for the reconstruction, therefore the distance between the two surfaces represents the inaccuracy of the reconstruction algorithm.

2.1. Experimental Setup

The experimental setup is shown in Fig. 2. The liver phantom used throughout the experiments was produced by the ARTORG centre and Cascination®. In addition to the phantom, 10 multimodality fiducial markers (IZI Medical Products®) were attached to the liver phantom in order to aid registration between the stereo surface reconstruction and the CT scan segmentation. An intra-operative CT (Artis Zeego, Siemens®) scan (DynaCT) of the liver phantom was performed with the phantom positioned on the surgical table (Fig. 2 (a)). A flex3D Olympus® stereo laparoscope camera was used to capture the stereo images in a laparoscopic
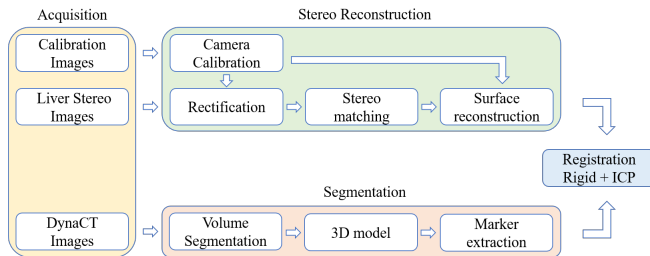

Figure 1. Workflow for registration of intra-operative reconstructed surface from stereo camera to surface extracted from DynaCT scan.
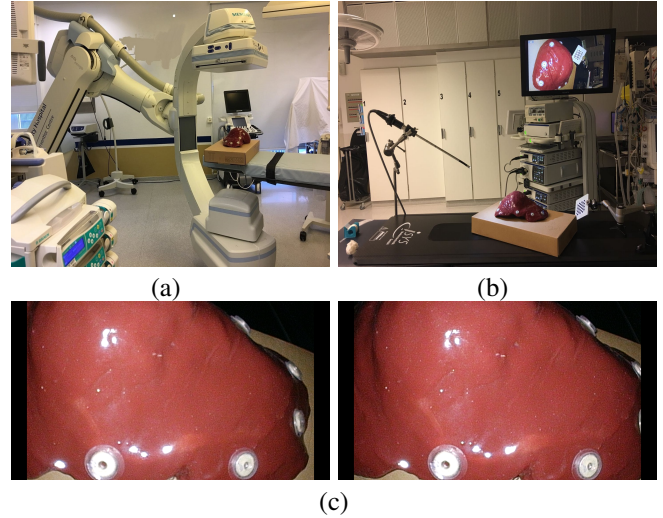

Figure 2. Illustration of the experimental setup. (a) DynaCT scan acquisition of the liver phantom; (b) Experimental setup for liver surface reconstruction; (c) Stereo images captures of the liver phantom.

Operating Room (OR) (Fig. 2 (b)). The stereo laparoscopic images were acquired using a DeckLink Duo® by BlackMagic Design, the stereo captures of the liver phantom can be seen in Fig. 2(c).

2.2. DynaCT Scan Segmentation

Segmentation of the liver phantom parenchyma was performed on 3D Slicer 4.6.2 through a combination of the *ThresholdEffect* and *LevelTracingEffect* modules. The label map, with a threshold of μ_1 = -201.98 [voxel intensity] was then used to create a model of the surface. A second segmentation was also performed, with a higher intensity of μ_2 = 841.34, to segment the markers. The marker centroids were successively separately classified through Fuzzy C-Means classification (FCM) and clustered to obtain a single position for each marker [13].

2.3. Stereo Surface Reconstruction

Prior to liver surface reconstruction, camera calibration was used to compute the intrinsic and extrinsic parameters of the stereo laparoscope camera. Calibration was performed based on Zhang's camera calibration algorithm [14] by a checkerboard pattern (Fig. 2 (b)). Calibration parameters were computed through a total of 26 calibration image pairs with an average reprojection error of 0.737 pixels. This camera calibration method was chosen because of its notoriety and extended use in the camera calibration community [14].

In order to lower the noise introduced by the background of the image, the stereo laparoscope camera images, shown in Fig. 2 (c), were segmented via the Graph Cut segmentation method [15]. This allowed to create a mask which only contained the liver surface and a background with zero average.

A dense intra-operative liver surface was reconstructed according to the algorithm proposed by Wang *et al.* in [8]. The algorithm first performs a global variational based disparity estimation method on the coarse pyramid level of the image based on gray level intensity and gradient constancy assumptions [16]. Successively, the low-resolution disparity map is up-sampled to the original scale. Triangulation technique [17] was used to generate the surface based on the disparity map.

Finally, to remove the effect of the background in the point cloud reconstructions, thresholding of the RGB channel at [50,50,50] of the cloud points was applied. This threshold value was chosen empirically. This additional thresholding allowed to partially remove some outliers which were due to masking of the stereo images.

2.4. Registration

The images of the liver phantom were acquired with the stereo camera at distances similar to those used for laparoscopic surgery (approximately at 5-10 cm from the liver). For this reason, the surface reconstruction could only reconstruct patches of the liver (parts of the liver included in the stereo images), and therefore not the entire liver surface, as visible in Fig. 3. For this reason, the registration between the segmented liver parenchyma and the reconstructed surface needed to be aided through the use of fiducial markers via point based registration [18]. The marker positions segmented from the camera images were reconstructed and registered to the marker centroids of the CT scan segmentation [19]. Finally, the registration between the CT scan point cloud and the reconstructed surface point cloud was further refined using Iterative Closest Point (ICP) registration between the two surfaces [18]. ICP was performed using a down sampled version (2%) of the reconstruction point clouds. An illustration of two registration results between the surface reconstruction and the CT is shown in Fig. 3.
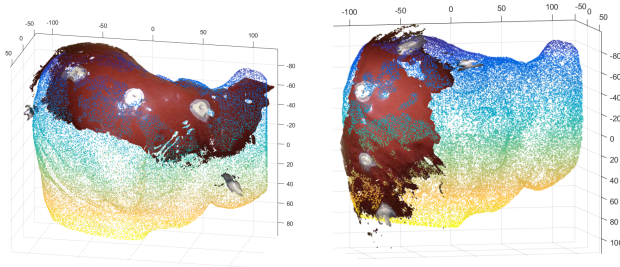

Figure 3. Surface reconstruction examples from single stereo images (red) rigidly registered to the CT scan segmentation (colour map). The error is represented by the distances between the two surfaces, with axes in [mm].

3. Results

A total of 30 stereo image pairs of the liver phantom were used for the performance evaluation of the reconstruction method using two common metrics, namely the Mean

Absolute Error (MAE) and Hausdorff distance. The data was divided into 2 datasets of 15 reconstructed point clouds. *Dataset1* encompasses 15 reconstructed point clouds of the liver phantom in its original configuration. *Dataset2* includes another set of 15 reconstruction surfaces after application of a deformation to the flexible liver phantom. Both reconstruction sets were associated to their respective CT scans used as ground truth for the 30 reconstructed surfaces.

The Mean Absolute Error ((MAE), Eq. (1)) between the registered liver surface $\hat{Y}$ and the liver parenchyma segmentation from the CT scan Y was computed as measure of accuracy for the registered points of the reconstruction surface and was calculated according to:

$$MAE = \sum_{(x,y,z)\in\Omega} \frac{1}{N} |\hat{Y}(x,y,z) - Y(x,y,z)|, \quad (1)$$

where N is the number of points, (x, y, z) denotes the 3D coordinates of the points, Y presents the surface point cloud extracted from CT scan and $\hat{Y}$ is the point cloud obtained by stereo vision reconstruction.
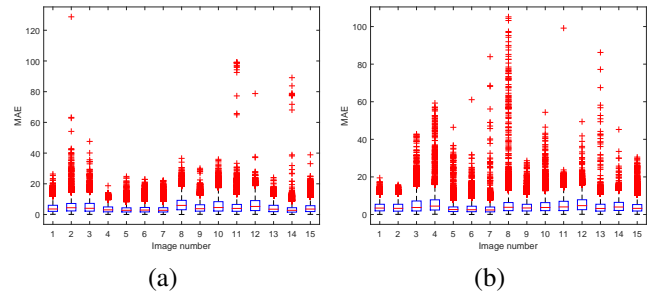

Figure 4. Box plot representation of the MAE between two surfaces $\hat{Y}$ and Y. (a) *Dataset1*; (b) *Dataset2*.

The MAE between corresponding points through ICP registration for both datasets are presented in the boxplots of Fig. 4. The mean of the MAE throughout the 30 reconstructed surfaces was found to be $\mu = 4.6$ mm (mean) for *Dataset1* and $\mu = 4.4$ mm (mean) for *Dataset2*.

As previously stated, only 2% of the reconstructed 3D points and points from CT were used for registration. The MAE therefore was only evaluated across 2% of the point clouds, which are also points used for registration. In order to evaluate the accuracy of the reconstruction on also other points of the reconstructed surface, *Hausdorff* distance was calculated, according to [20]:

$$H(A,B) = max(h(A,B), h(B,A)), \quad (2)$$

where A is the reconstructed point cloud and B represents the point cloud from CT scan. The function $h(A, B)$ is known as directed Hausdorff distance and is defined by:

$$h(A,B) = \max_{a\in A} \min_{b\in B} ||a - b||, \quad (3)$$

where $|| \cdot ||$ denotes the Euclidean norm of the pointwise distances, a denotes a single point from the point cloud A and b is a single point from B.
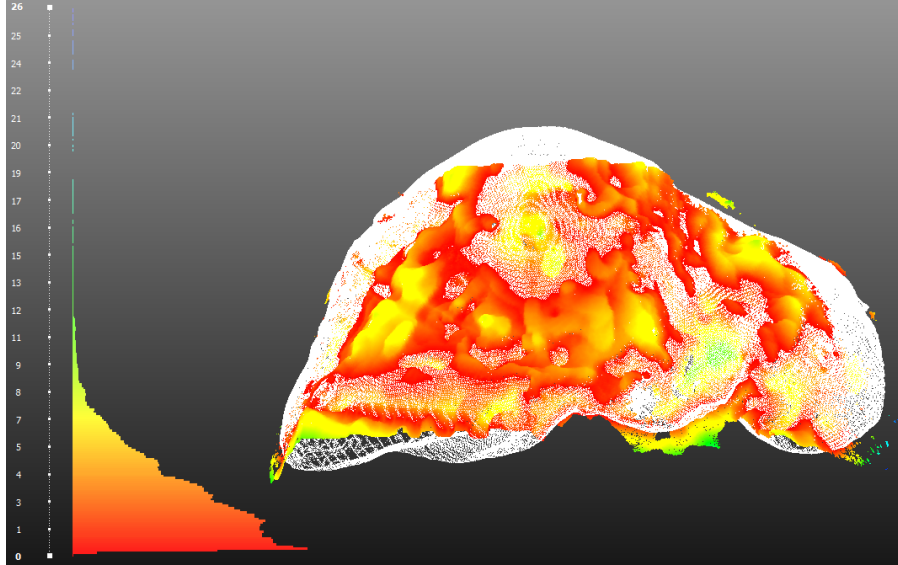
Figure 5. Example of Hausdorff distance error map. The reconstructed distance map is represented through the colormap, whereas the CT scan segmentation is the white point cloud. The histogram on the left side denotes error for each point in the reconstruction (error in [mm]), the closer the two surfaces, the lower the error. Average distance of 3.3 mm, although outliers in blue colour appear with a Hausdorff distance of 26 mm.

Meshlab® was used to compute unidirectionally the Hausdorff distance to the CT scan following the implementation presented in [21]. In Fig. 5, one of the results of the Hausdorff distance map is presented. The CT scan segmented surface is illustrated as a white point cloud, whereas the Hausdorff distance map is plotted in colormap, where red intensity defines proximity of the surfaces and blue indicates higher error values. The quality histogram label map bar in the left side of the image denotes distribution of the error. Most of the reconstructed points achieve a low error, while there are some outliers which have high error values, similarly to what was found through MAE.

TABLE 1. MAE AND HAUSDORFF IN [MM] IN TERMS OF MEAN μ, STANDARD DEVIATION σ AND MAXIMA FOR *Dataset1* AND *Dataset2*.

	Dataset1	*Dataset2*
MAE ($\mu \pm \sigma$)	4.6±1.0	4.4 ± 0.8
max_{MAE}	128.8	105.2
Hausdorff ($\mu \pm \sigma$)	3.7±0.8	3.6 ± 0.8
max_H	78.5	106.6

4. Discussion

The surface reconstruction approach presented in [8] relies on the intensity and gradient values of the whole image for stereo image reconstruction. Tab. 1 shows the mean, variance and maxima values for both measures of evaluation, MAE and Hausdorff distance. Overall, MAE and Hausdorff distances show that the reconstruction method proposed in [8] currently performs accurate reconstructions in the order of 3 or 4 mm.

From Fig. 4, the results show an accurate reconstruction of the liver surface through single stereo image pairs. However, a large presence of outliers is also visible in Fig. 4. These are either due to errors which are introduced inevitably through triangulation steps, as pointed out in [11], or to outliers created by the segmentation and reconstruction algorithm. Through image processing methods, the outliers could be lowered greatly. This holds especially those caused by incorrect segmentation of the stereo images. The outliers present are also due to artefacts such as light reflection (on the surface), which causes large incorrect peaks in the reconstructed surface. These effects can be reduced through image enhancement techniques such as [22].

Moreover, other sources of noise in the reconstruction include the image quality of the flexible stereo laparoscope camera used for this study. It presents noisy images and therefore affects the smoothness of the image reconstruction. Testing should be performed with other stereo laparoscope cameras through multiple image acquisition methods.

Segmentation of the liver surface from CT scan also introduces errors in the ground truth data. Firstly, this is due to inaccuracies inherent to the CT scanner itself. Secondly, the process of volume segmentation also creates smooth models which do not replicate the exact texture and surface of the liver phantom itself and therefore provides an incorrect ground truth. Inaccuracy in the registration through markers could be improved using smaller markers, which would consequently lead the ICP registration to a more accurate solution and a better definition of the error.

To understand the true value of this reconstruction algorithm for image guided surgery, expansion of the reconstructed surface should be performed through computer vision algorithms, such as surface stitching. This will allow the reconstruction to cover the full surface of the liver.

5. Conclusion

This study describes a simulation setup and validation of a surface reconstruction method based on stereo vision with application to image guided laparoscopic liver resection surgery. The tests were performed using available equipment in OR based on conventional approaches for planned laparoscopic liver resection surgery. The surface reconstruction was performed on a liver phantom which represents human anatomy. Conclusion of the study was that the approach for the reconstruction through stereo camera, according to the method proposed in [8], is valid.

The aim of the surface reconstruction method will be to improve the accuracy of image guided surgery, through automatic processes of registration of volumetric data, such as CT and MRI, to the laparoscopic perspective. This will allow the surgeon to visualize structures hidden underneath the surface, such as blood vessels, or surgical planning resection planes [23], directly overlayed on top of the camera perspective. In order to improve the reconstruction algorithm according to the problems described in Section 4, the reconstruction method will be combined with computer vision algorithms such as hand-eye calibration for camera image tracking subsequent stitching algorithms. The validity of the algorithm will be further explored and tested in a surgical environment, in order to understand its accuracy in a clinical scenario.

6. Acknowledgements

References

[1] K. Cleary and T. M. Peters, "Image-guided interventions: technology review and clinical applications," *Annual review of biomedical engineering*, vol. 12, pp. 119–142, 2010.

[2] R. Palomar, F. Alaya Cheikh, B. Edwin, A. Beghdadi, and O. J. Elle, "Surface reconstruction for planning and navigation of liver resections," *Computerized Medical Imaging and Graphics*, vol. 53, pp. 30–42, 2016.

[3] J. S. Heiselman, L. W. Clements, J. A. Collins, J. A. Weis, A. L. Simpson, S. K. Geevarghese, T. P. Kingham, W. R. Jarnagin, and M. I. Miga, "Characterization and correction of intraoperative soft tissue deformation in image-guided laparoscopic liver surgery," *Journal of Medical Imaging*, vol. 5, no. 2, p. 021203, 2017.

[4] L. Maier-Hein, P. Mountney, A. Bartoli, H. Elhawary, D. Elson, A. Groch, A. Kolb, M. Rodrigues, J. Sorger, S. Speidel *et al.*, "Optical techniques for 3d surface reconstruction in computer-assisted laparoscopic surgery," *Medical image analysis*, vol. 17, no. 8, pp. 974–996, 2013.

[5] L. Chen, W. Tang, N. W. John, T. R. Wan, and J. J. Zhang, "Slam-based dense surface reconstruction in monocular minimally invasive surgery and its application to augmented reality," *Computer Methods and Programs in Biomedicine*, 2018.

[6] F. Devernay, F. Mourgues, and È. Coste-Manière, "Towards endoscopic augmented reality for robotically assisted minimally invasive cardiac surgery," in *International Workshop on Medical Imaging and Augmented Reality*. IEEE, 2001, pp. 16–20.

[7] D. Stoyanov, M. V. Scarzanella, P. Pratt, and G.-Z. Yang, "Real-time stereo reconstruction in robotically assisted minimally invasive surgery," in *International Conference on Medical Image Computing and Computer-Assisted Intervention*. Springer, 2010, pp. 275–282.

[8] C. Wang, F. Cheikh Alaya, M. Kaaniche, and O. J. Elle, "Liver surface reconstruction for image guided surgery," in *Medical Imaging 2018: Image-Guided Procedures, Robotic Interventions, and Modeling*, vol. 10576. International Society for Optics and Photonics, 2018, p. 105762H.

[9] L. Maier-Hein, A. Groch, A. Bartoli, S. Bodenstedt, G. Boissonnat, P.-L. Chang, N. Clancy, D. S. Elson, S. Haase, E. Heim *et al.*, "Comparative validation of single-shot optical techniques for laparoscopic 3-d surface reconstruction," *IEEE transactions on medical imaging*, vol. 33, no. 10, pp. 1913–1930, 2014.

[10] S. Suwelack, S. Röhl, S. Bodenstedt, D. Reichard, R. Dillmann, T. Santos, L. Maier-Hein, M. Wagner, J. Wünscher, H. Kenngott *et al.*, "Physics-based shape matching for intraoperative image guidance," *Medical physics*, vol. 41, no. 11, 2014.

[11] S. Thompson, J. Totz, Y. Song, S. Johnsen, D. Stoyanov, S. Ourselin, K. Gurusamy, C. Schneider, B. Davidson, D. Hawkes *et al.*, "Accuracy validation of an image guided laparoscopy system for liver resection," in *Medical Imaging 2015: Image-Guided Procedures, Robotic Interventions, and Modeling*, vol. 9415. International Society for Optics and Photonics, 2015, p. 941509.

[12] J. S. Heiselman, J. A. Collins, L. W. Clements, J. A. Weis, A. L. Simpson, S. K. Geevarghese, W. R. Jarnagin, and M. I. Miga, "Emulation of the laparoscopic environment for image-guided liver surgery via an abdominal phantom system with anatomical ligamenture," in *Medical Imaging 2017: Image-Guided Procedures, Robotic Interventions, and Modeling*, vol. 10135. International Society for Optics and Photonics, 2017, p. 101352W.

[13] J. C. Bezdek, R. Ehrlich, and W. Full, "Fcm: The fuzzy c-means clustering algorithm," *Computers & Geosciences*, vol. 10, no. 2-3, pp. 191–203, 1984.

[14] Z. Zhang, "A flexible new technique for camera calibration," *IEEE Transactions on pattern analysis and machine intelligence*, vol. 22, no. 11, pp. 1330–1334, 2000.

[15] Y. Li, J. Sun, C.-K. Tang, and H.-Y. Shum, "Lazy snapping," in *ACM Transactions on Graphics (ToG)*, vol. 23, no. 3. ACM, 2004, pp. 303–308.

[16] T. Brox, A. Bruhn, N. Papenberg, and J. Weickert, "High accuracy optical flow estimation based on a theory for warping," *Computer Vision-ECCV 2004*, pp. 25–36, 2004.

[17] G. Bradski and A. Kaehler, *Learning OpenCV: Computer vision with the OpenCV library*. " O'Reilly Media, Inc.", 2008.

[18] P. J. Besl and N. D. McKay, "Method for registration of 3-d shapes," in *Sensor Fusion IV: Control Paradigms and Data Structures*, vol. 1611. International Society for Optics and Photonics, 1992, pp. 586–607.

[19] K. S. Arun, T. S. Huang, and S. D. Blostein, "Least-squares fitting of two 3-d point sets," *IEEE Transactions on pattern analysis and machine intelligence*, no. 5, pp. 698–700, 1987.

[20] D. P. Huttenlocher, G. A. Klanderman, and W. J. Rucklidge, "Comparing images using the hausdorff distance," *IEEE Transactions on pattern analysis and machine intelligence*, vol. 15, no. 9, pp. 850–863, 1993.

[21] P. Cignoni, C. Rocchini, and R. Scopigno, "Metro: measuring error on simplified surfaces," in *Computer Graphics Forum*, vol. 17, no. 2. Blackwell Publishers, 1998, pp. 167–174.

[22] D. Stoyanov and G. Z. Yang, "Removing specular reflection components for robotic assisted laparoscopic surgery," in *Image Processing, 2005. ICIP 2005. IEEE International Conference on*, vol. 3. IEEE, 2005, pp. III–632.

[23] R. Palomar, F. Alaya Cheikh, B. Edwin, Å. Fretland, A. Beghdadi, and O. J. Elle, "A novel method for planning liver resections using deformable bézier surfaces and distance maps," *Computer methods and programs in biomedicine*, vol. 144, pp. 135–145, 2017.